J|A|C|S ARTICLES

Published on Web 01/22/2009

Mapping NO Movements in Crystalline [Fe(Porph)(NO)(1-MeIm)]

Nathan J. Silvernail,[†] Alexander Barabanschikov,[‡] J. Timothy Sage,[‡] Bruce C. Noll,[†] and W. Robert Scheidt*,[†]

Department of Chemistry and Biochemistry, University of Notre Dame, Notre Dame, Indiana 46556, and Department of Physics and Center for Interdisciplinary Research on Complex Systems, Northeastern University, Boston, Massachusetts 02115

Received July 17, 2008; E-mail: Scheidt.1@nd.edu

Abstract: Orientational disorder of the distal nitrosyl (NO) ligand in iron porphyrinates is a common phenomenon. We present an analysis of multitemperature crystallographic data for the order/disorder phenomenon. The observed temperature-dependent order/disorder and variable rotational orientations of nitrosyl ligands for six different six-coordinate iron porphyrinates have been examined in terms of the nonbonded contacts found in the solid state. Favorable orientations for NO can be identified either by calculation of the close nonbonded contacts or by evaluation of the geometry-dependent potential energy using semiempirical nonbonded potential functions. The nonbonded contacts display temperature-dependent differences consistent with observed structural differences. The motion of NO appears to be controlled by intermolecular interactions that allow a limited set of orientations, and under some conditions, only a single NO orientation is allowed. In some cases, the equilibria involving the orientations of NO can be analyzed using the van't Hoff relationship, and the free energy and enthalpy of the solid-state transitions can be evaluated. The intrinsic barriers to rotation of the NO were examined using a fine-meshed series of DFT calculations. The calculations also showed the detailed effects of the variation of the NO orientation on the equatorial bond distances.

Introduction

The binding of the diatomic ligands O_2, CO, and NO to heme proteins is an area of longstanding interest in bioinorganic chemistry.[1] Initially, the interest in these ligands was in understanding the basis for the reduced binding affinity of CO relative to O_2 in the oxygen-binding/carrying proteins myoglobin (Mb) and hemoglobin. Specific interactions of the Fe−O_2 adduct with amino acid residues in the ligand binding pocket have been suggested to play an important role in the stabilization of the Fe−O_2 complex in hemoglobin and myoglobin and subsequently aid in the small-molecule specificity of the protein.[2] A prominent early idea was that the environment of the protein ligand binding pocket imposes constraints on the Fe−C−O unit but not on the Fe−O−O unit. It is apparent that the ligand binding pockets in proteins such as myoglobin and hemoglobin are somewhat more constraining for the linear Fe−C−O unit than for the angular Fe−O−O unit.

Indeed, many crystal structures, especially the earlier ones, suggested that the Fe−C−O unit was bent and/or tilted,[3] and it was concluded that this unusual geometry was a response to the constraints of the ligand binding pocket. Despite the attractiveness of this proposal, the energetic costs of such distortions from idealized geometry were often cited as making this explanation unlikely. More recent protein structures have an Fe−C−O angle of $\geq 160°$.[4] However, DFT calculations by Ghosh and Bocian[5] suggest that a cooperative bend/tilt distortion is of relatively low energy and that its contribution to the total binding energy is relatively small. It is clear, however, that more general steric interactions play a role in the movement of bound ligands and ligands in and near the distal (ligand binding) pocket. The frequent presence of multiple conformations in liganded myoglobins[4a] also reveals the complexities. Some of these motions have been thoroughly investigated by studying photodissociation/geminate recombination of CO in MbCO.

Photodissociation of CO from MbCO leads to motion of the ligand toward the Xe4 site.[6] This suggested pathway of diatomic ligand ejection is defined by the amino acid residues valine and phenylalanine that flank the binding pocket and a histidine opposite the Xe4 site.[6] This well-defined pocket has been investigated by studying the time-dependent crystal structure of the CO-bound adduct after photodissociation. From these investigations, a well-defined volume with sufficient room for CO after photolysis has been described. In all of these studies,

[†] University of Notre Dame.
[‡] Northeastern University.

(1) *The Smallest Biomolecules: Diatomics and Their Interactions with Heme Proteins*; Ghosh, A., Ed.; Elsevier: Amsterdam, 2008.
(2) (a) Olson, J. S.; Phillips, G. N., Jr *J. Biol. Inorg. Chem.* **1997**, *2*, 544. (b) Rohlfs, R. J.; Mathews, A. J.; Carver, T. E.; Olson, J. S.; Springer, B. A.; Egeberg, K. D.; Sligar, S. G. *J. Biol. Chem.* **1990**, *265*, 3168.
(3) (a) Kuriyan, J.; Wilz, S.; Karplus, M.; Petsko, G. *J. Mol. Biol.* **1986**, *192*, 133. (b) Cheng, X.; Schoenborn, B. P. *J. Mol. Biol.* **1991**, *220*, 381.
(4) (a) Vojtěchovský, J.; Chu, K.; Berendzen, J.; Sweet, R. M.; Schlichting, I. *Biophys. J.* **1999**, *77*, 2153. (b) Kachalova, G. S.; Popov, A. N.; Bartunik, H. D. *Science* **1999**, *284*, 473.
(5) (a) Ghosh, A.; Bocian, D. F. *J. Phys. Chem.* **1996**, *100*, 6363. (b) Vangberg, T.; Bocian, D. F.; Ghosh, A. *J. Biol. Inorg. Chem.* **1997**, *2*, 526.

 © 2009 American Chemical Society

the CO is found to migrate toward the Xe4 site, opposite histidine-64. Additionally, this defines the volume that is just appropriate for the binding of the angular ligands NO and O_2.

More recently, a number of heme protein families that function as diatomic molecule sensors have been discovered and characterized. These sensor systems have often developed discrimination between the diatomic ligand that functions as the biological messenger and other diatomics that effectively can be a noisy background.[7] Nitric oxide (NO)[8] coordinates to several heme proteins, causing a number of physiological responses. NO acts as a signaling molecule that has been implicated in a number of fundamental processes, including smooth-muscle relaxation,[9,10] platelet deaggregation,[11] neuronal communication,[12] aspects of myocardial function, and numerous other physiological functions.[13]

Among the more intriguing systems are those that discriminate between NO and O_2. The most widely studied of these is mammalian soluble guanylyl cyclase (sGC), which effectively coordinates NO but strongly discriminates against the binding of O_2. This discrimination occurs despite the similar bent (Fe−X−O) bonding configuration of NO and O_2. The specificity of NO over O_2 binding is thought to possibly arise from specific amino acid residue interactions leading either to stabilization of the Fe−NO bond but not the Fe−O_2 bond or interactions leading to a destabilization of the Fe−O_2 bond.[14] On the other hand, genomic analysis of sGC has led to the identification of multiple prokaryotic proteins with similar sites.[15] At least some of these are known to have spectroscopic properties, sequence homology, and conserved residues similar to those of sGC. These prokaryotic proteins have different roles than sGC, and some, but not all, bind O_2, whereas others bind NO much like sGC. The possible differences are suggested by the acronyms of some of these: SONO (sensor of NO),[16] HNOX (heme−nitric oxide/oxygen),[17] and NOB (nitric oxide binder).[15] Interestingly, only O_2 complexes of proteins of this class have been structurally characterized.[16,18]

The differences between the binding geometries of NO and O_2 as opposed to CO in the iron porphyrinates has led to the result that only the carbonyl species display ordered structures. The angular geometry of Fe−NO and Fe−O_2 has led to iron porphyrinate structures in which the O_2 or NO ligand is disordered and displays multiple rotational positions around the Fe−O[19,20] or Fe−N[21,22] bond, respectively. The origin of the observed structural disorder in the O_2 complexes clearly originates in the crystalline environment of the ligand, and both static and dynamic disorder of the Fe−O_2 group are claimed.[19,23]

Recent structural studies of the six-coordinate NO derivatives [Fe(T*p*XPP)(NO)(1-MeIm)] (X = F, OCH_3)[8] demonstrated three totally ordered NO-ligated complexes. Perhaps surprisingly, although the crystal structure analyses showed that all three of these nitrosyl species are completely ordered at 100 K, additional orientations of NO were observed at higher temperatures.[24] This thermally driven rotational disorder appears to be completely reversible. Each disordered system showed distinct orientational and thermal features, all related to the crystalline environment around the NO binding site. All of the nitrosyl systems must be dynamically disordered, and moreover, they provide a unique opportunity to study structurally based orientational discrimination.

We have examined the intermolecular interactions (nonbonded distances) involving NO as a function of the rotation of NO about the Fe−N axis. This analysis shows that each system has regions in which the intermolecular interactions between NO and the surrounding molecules are small and favor the location of NO and other regions where these interactions are large and disfavor the location of NO. In some cases, there is a obvious barrier to the rotation of NO from one region to the other, whereas in others, the definition between orientations is less apparent.

We have mapped the systems first by finding all of the intermolecular contacts involving NO that are smaller than the sum of the van der Waals radii and summing the differences. The larger the total difference sum, the less favorable is a possible NO orientation. A second analysis calculating the semiempirical nonbonded potential function for possible NO orientations was also made,[25,26] and an evaluation of the possible differences between the approaches is given. In addition to the three temperature-dependent systems noted above, we have collected new structural data on [Fe(TPP)(NO)(1-MeIm)], which

(6) (a) Schlichting, I.; Berendzen, J.; Phillips, G. N., Jr.; Sweet, R. M. *Nature* **1994**, *371*, 808. (b) Hartmann, H.; Zinser, S.; Komninos, P.; Schneider, R. T.; Nienhaus, G. U.; Parak, F. *Proc. Natl. Acad. Sci. U.S.A.* **1996**, *93*, 7013. (c) Teng, T.-Y.; Šrajer, V.; Moffat, K. *Biochemistry* **1997**, *36*, 12087.

(7) Gilles-Gonzalez, M.-A.; Gonzalez, G. In *The Smallest Biomolecules: Diatomics and Their Interactions with Heme Proteins*; Ghosh, A., Ed.; Elsevier: Amsterdam, 2008; Chapter 2.

(8) The following abbreviations are used in this paper: NO, nitric oxide; *mono*-[Fe(T*p*FPP)(NO)(1-MeIm)], monoclinic form of (1-methylimidazole)(nitrosyl)*meso*-(*para*-fluorotetraphenylporphyrinato)iron; *tri*-[Fe(T*p*FPP)(NO)(1-MeIm)], triclinic form of (1-methylimidazole)(nitrosyl)*meso*-(*para*-fluorotetraphenylporphyrinato)iron; Porph, generalized porphyrin dianion; T*p*OCH_3PP, *meso*-*para*-methoxytetraphenylporphyrin; T*p*CF_3PP, *meso*-*para*-trifluoromethyltetraphenylporphyrin; T*p*NO_2PP, *meso*-*para*-nitrotetraphenylporphyrin; TPP, dianion of *meso*-tetraphenylporphyrin; His, histidine; 1-MeIm, 1-methylimidazole.

(9) Rapoport, R. M.; Murad, F. *Circ. Res.* **1983**, *52*, 352.

(10) Ignarro, L. J.; Adams, J. B.; Horwitz, P. M.; Wood, K. S. *J. Biol. Chem.* **1986**, *261*, 4997.

(11) (a) Azuma, H.; Ishikawa, M.; Sekizaki, S. *Br. J. Pharmacol.* **1986**, *88*, 411. (b) Furlong, B.; Henderson, A. H.; Lewis, M. J.; Smith, J. A. *Br. J. Pharmacol.* **1987**, *90*, 687. (c) Radomski, M. W.; Palmer, R. M. J.; Moncada, S. *Br. J. Pharmacol.* **1987**, *92*, 639.

(12) Garthwaite, J. *Trends Neurosci.* **1991**, *14*, 60.

(13) Koshland, D. E., Jr *Science* **1992**, *258*, 1861. Butler, A. R.; Williams, D. L. H. *Chem. Soc. Rev.* **1993**, 233. Moncada, S.; Palmer, R. M. J.; Higgs, E. A. *Pharmacol. Rev.* **1991**, *43*, 109.

(14) Sousa, E. H. S.; Gonzalez, G.; Gilles-Gonzalez, M.-A. In *The Smallest Biomolecules: Diatomics and Their Interactions with Heme Proteins*; Ghosh, A., Ed.; Elsevier: Amsterdam, 2008; pp 534−535.

(15) Iyer, L. M.; Anantharaman, V.; Aravind, L. *BMC Genomics* **2003**, *6*, 490.

(16) Nioche, P.; Berka, V.; Vipond, J.; Minton, N.; Tsai, A. L.; Raman, C. S. *Science* **2004**, *306*, 1550.

(17) Karow, D, S.; Pan, D.; Tran, R.; Pelllicena, P.; Presely Mathies, R. A.; Marletta, M. A. *Biochemistry* **2004**, *43*, 10203.

(18) Pellicena, P.; Karow, D. S.; Boon, E. M.; Marletta, M. A.; Kuriyan, J. *Proc. Natl. Acad. Sci. U.S.A.* **2004**, *101*, 12854.

(19) Schappacher, M.; Ricard, L.; Fischer, J.; Weiss, R.; Bill, E.; Montiel-Montoya, R.; Winkler, H.; Trautwein, A. X. *Eur. J. Biochem.* **1987**, *168*, 419.

(20) (a) Jameson, G. B.; Rodley, G. A.; Robinson, W. T.; Gagne, R. R.; Reed, C. A.; Collman, J. P. *Inorg. Chem.* **1978**, *17*, 850. (b) Jameson, G. B.; Molinaro, F. S.; Ibers, J. A.; Collman, J. P.; Brauman, J. I.; Rose, E.; Suslick, K. S. *J. Am. Chem. Soc.* **1980**, *102*, 3224.

(21) Scheidt, W. R.; Piciulo, P. L. *J. Am. Chem. Soc.* **1976**, *98*, 1913.

(22) Wyllie, G. R. A.; Schulz, C. E.; Scheidt, W. R. *Inorg. Chem.* **2003**, *42*, 5722.

(23) (a) Spartalian, K.; Lang, G.; Collman, J. P.; Gagne, R. R.; Reed, C. A. *J. Chem. Phys.* **1975**, *63*, 5375. (b) Godbout, N.; Sanders, L. K.; Salzmann, R.; Havlin, R. H.; Wojdelski, M.; Oldfield, E. *J. Am. Chem. Soc.* **1999**, *121*, 3829.

(24) Silvernail, N. J.; Pavlik, J. W.; Noll, B. C.; Schulz, C. E.; Scheidt, W. R. *Inorg. Chem.* **2008**, *47*, 912.

(25) Giglio, E. *Nature* **1969**, *222*, 339.

(26) Shmueli, U.; Goldberg, I. *Acta Crystallogr.* **1973**, *B29*, 2466.

is known to be disordered at both low and ambient temperature,[21,22] and two additional six-coordinate nitrosyl complexes. Maps of the solid-state interaction landscape may be used in a predictive manner to find the most likely position of additional NO orientations. This predictive utility is found even for the landscapes from the low-temperature structures, where there is little or no disorder. This technique has been used on a total of six different complexes to develop strategies for exploring the orientation of NO ligands in the solid state. Thus, a total of six different nitrosyl iron porphyrinate systems have been analyzed by the above methods. The method was also used to examine the interactions in the ligand binding pocket for two different reported nitrosylmyoglobin derivatives.

Finally, we have used density functional theory (DFT) methods to study the intrinsic barriers to rotation in [Fe(porphine)(NO)(1-MeIm)]. These have provided an indication of the intramolecular contributions to the rotation barriers. The calculations have also provided a full analysis of the effect of rotation on heme iron bonding parameters. This analysis further demonstrates how a seemingly simple molecule, NO, can have strong influences on heme coordination chemistry. These experimental and computational studies along with investigations of analogous O_2 movements[27] are expected to provide further information on discrimination differences between diatomic O_2 and NO.

Experimental Section

Synthesis of [Fe(Porph)(NO)(1-MeIm)]. [Fe(T*p*CF_3PP)(NO)(1-MeIm)] and [Fe(T*p*NO_2PP)(NO)(1-MeIm)] were synthesized using methods similar to those reported elsewhere.[24] [Fe(TPP)(NO)(1-MeIm)] was synthesized using a previously reported procedure.[21,22]

X-ray Crystallographic Studies. Crystal data were collected and integrated using a Bruker x8 or D8 Apex II system with graphite-monochromatized Mo Kα radiation ($\lambda = 0.71073$ Å) at 100 and 293 K (700 Series Oxford Cryostream).[28] The programs SADABS[30] and TWINABS[31] were applied for absorption correction. All of the structures were solved using the Patterson method in XS[32] and refined using XL.[33] The population of the NO oxygen orientations in each of the 23 structures were also established during the structure refinement routine using XL.[33] All of the atoms were found after successive full-matrix least-squares refinement cycles on F^2 and refined with anisotropic thermal parameters. Hydrogen atoms were placed at calculated geometries and allowed to ride on the positions of the parent atoms. Thermal parameters for non-methyl and methyl hydrogens were respectively set to 1.2 and 1.5 times the equivalent isotropic U values of the parent atoms.

Solid-state analysis of crystal packing distances made use of the program MERCURY[34] from the Cambridge Crystallographic Data Centre.

Theoretical calculations were performed using DFT as implemented in Gaussian 03,[35] employing the B3LYP[36] hybrid functional and Ahlrich's VTZ[37] basis set for the Fe atom and the 6-31G* basis set for all other atoms.

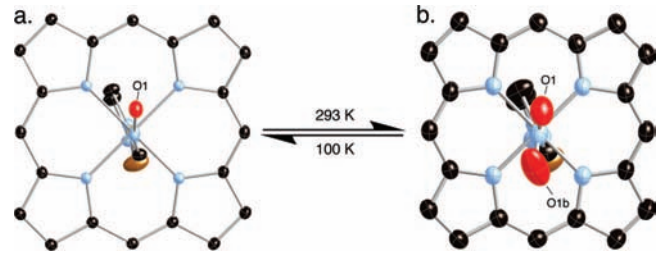

Figure 1. ORTEP diagrams (50% probability ellipsoids) of *tri*-[Fe(T*p*F-PP)(NO)(1-MeIm)] at (a) 100 and (b) 293 K. The molecules are oriented with the porphyrin plane in the page to emphasize the orientations of the NO oxygen. Hydrogen atoms and phenyl rings have been omitted for clarity. As a point of reference, the imidazole methyl group is always directed toward the bottom of the figures and is shown as a brown atom.

Results and Discussion

Figure 1 displays the strikingly different dispositions of the axial NO in *tri*-[Fe(T*p*FPP)(NO)(1-MeIm)]. The 100 K structure represented the first ordered nitrosyl ligand found in six-coordinate derivatives.[24] The two structures in Figure 1 were obtained on the same crystal; subsequent studies demonstrated that it is an equilibrium system in the solid state. The positions of the two oxygen atoms require a large (~180°) rotation about the Fe−N_{NO} bond. Thus, the oxygen motion required to achieve the ordered structure at 100 K from the crystal at 293 K is substantial. This represents the largest possible solid-state motion for a bound NO ligand, making this system especially appealing for study, and the unusual features of this system led us to study it intensively. The studies of *tri*-[Fe(T*p*FPP)(NO)(1-MeIm)] utilized two crystalline specimens and several temperatures with different cooling and heating regimes that have been described previously.[24] Figure 4 of ref 24 presents the 10 different structures determined. We concluded from these detailed crystal structure analyses that the system changes are both reproducible and reversible. NO populations were evaluated by least-squares refinements of the crystallographic data at the various temperatures.

As Figure 1 shows, the thermal motion suggests well-defined positions of oxygen at the two temperatures; either a specific bonding effect or specific environmental effects could lead to such well-defined positions. As discussed later, we do not think that bonding effects play a strong role in defining the relative NO orientation.

Environmental effects in the form of contacts close to the oxygen atom position were next examined. Intra- and intermolecular nonbonded oxygen contacts were examined with the program MERCURY.[34] Interatomic distances were compared with the sum of the van der Waals radii of the two atoms (values

(27) Li, J.-F.; Nair, S.; Noll, B. C.; Oliver, A. G.; Schulz, C. E.; Scheidt, W. R. Work in progress. An analysis of the apparent disorder of the dioxygen species is more complex than that of the NO species. The multiple positions of the terminal oxygen atom in the bent FeO_2 group in several crystal structures currently under study appears to reflect both disorder and crystallographic problems related to unresolved twinning.

(28) The Oxford control unit was calibrated at the factory using the phase change of Rochelle's salt at 109 K.[29] The factory calibration was checked in our laboratory with an iron−constantan thermocouple and an Omega 199 temperature meter. All of the reported temperatures are believed to be accurate to within 2 K.

(29) Tomaszewski, P. E. *Phase Trans.* **1992**, *38*, 127.

(30) Sheldrick, G. M. *SADABS*; Universität Göttingen: Göttingen, Germany, 2006.

(31) Sheldrick, G. M. *TWINABS*; Universität Göttingen: Göttingen, Germany, 2006.

(32) (a) Sheldrick, G. M. *XS*; Bruker-Nonius AXS: Madison, WI, 2001. (b) Patterson, A. L. *Phys. Rev.* **1934**, *46*, 372.

(33) Sheldrick, G. M. *Acta Crystallogr.* **2008**, *A64*, 112.

(34) (a) Macrae, C. F.; Edgington, P. R.; McCabe, P.; Pidcock, E.; Shields, G. P.; Taylor, R.; Towler, M.; van de Streek, J. *J. Appl. Crystallogr.* **2006**, *39*, 453. (b) Bruno, I. J.; Cole, J. C.; Edgington, P. R.; Kessler, M. K.; Macrae, C. F.; McCabe, P.; Pearson, J.; Taylor, R. *Acta Crystallogr.* **2002**, *B58*, 389. (c) Taylor, R.; Macrae, C. F. *Acta Crystallogr.* **2001**, *B57*, 815.

(35) Frisch, M. J.; et al. *Gaussian 03*, revision C.02; Gaussian, Inc.: Wallingford, CT, 2004.

(36) Becke, A. D. *J. Chem. Phys.* **1993**, *98*, 5684. Lee, C.; Yang, W.; Parr, R. G. *Phys. Rev. B* **1988**, *37*, 785.

(37) Schafer, A.; Horn, H.; Ahlrich, R. *J. Phys. Chem.* **1992**, *97*, 2571.

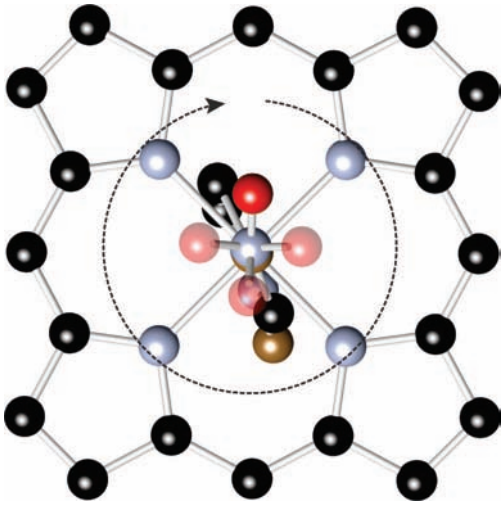

Figure 2. Schematic diagram displaying the rotation of nitrosyl oxygen parallel to the porphyrin plane, based on the 100 K results for *tri*-[Fe(T*p*FPP)(NO)(1-MeIm)]. The solid red ball shows the observed position, whereas the translucent red spheres represent calculated positions 90, 180, and 270° from the original. The methyl group of the trans 1-MeIm ligand has been colored brown for ease of recognition.

of the van der Waals radii were taken from ref 38). When the observed distance between the atom pairs was less than the sum of the van der Waals radii, the difference was recorded. The sum of all these differences was recorded as the "sum of the van der Waals radii overlaps" (*svdWro*), which can be considered as one measure of the importance of the nonbonded contacts. There are no *intra*molecular contacts to the oxygen atom that are less than the sum of the van der Waals radii. Thus, the oxygen positions are controlled solely by the *inter*molecular nonbonded interactions, which are sometimes called "crystal-packing effects". Such effects are often cited as the explanation of stereochemical features, and this system appears to provide an opportunity for a quantitative study of crystal packing.

The sum of the nonbonded contacts (i.e., the *svdWro* value) at the single oxygen atom position at 100 K and the second position at 293 K are small. We have evaluated the *svdWro* values for *tri*-[Fe(T*p*FPP)(NO)(1-MeIm)] at alternative positions of the oxygen atom by calculating the crystal coordinates of this atom as it is rotated around a circle parallel to the porphyrin plane at a constant bond distance from the nitrosyl nitrogen. This is schematically shown in Figure 2, where the observed oxygen position[39] is shown in red and the positions of the oxygen atom at positions 90, 180, and 270° from the original position are shown as translucent red spheres. The *svdWro* values were evaluated for a total of 36 positions around this circle. Because of the potential interest in the relative orientation of the FeNO group and the trans imidazole ligand, we defined an NO coordinate rotation system in which the rotation angle has the value 0° when the FeNO and imidazole planes are coplanar and the methyl group and the oxygen are "pointing" in the same direction. With that definition, the observed position of the nitrosyl group is either −154 or 206°, as shown in Figure 2, and the displayed alternative positions have rotation angles of 26, 116, and 296°.

We have plotted the *svdWro* values as a function of the 36 oxygen atom positions for *tri*-[Fe(T*p*FPP)(NO)(1-MeIm)] at both

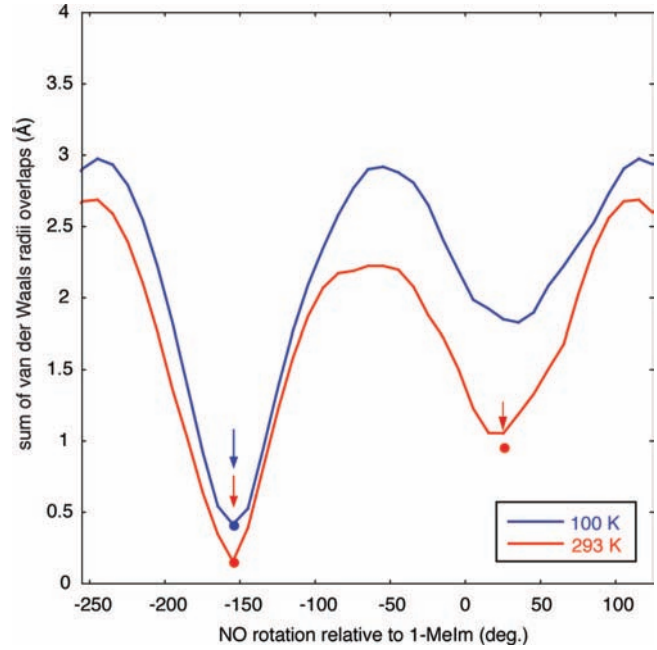

Figure 3. Sum of the van der Waals radii overlaps (Å) at 100 and 293 K vs the rotation of NO oxygen for *tri*-[Fe(T*p*FPP)(NO)(1-MeIm)]. These values are periodic (360° repeat). This plot provides a measure of the unfavorable intermolecular nonbonded oxygen interactions. The observed positions and *svdWro* values of the oxygen atom at the two temperatures are shown as points and indicated by arrows.

100 and 293 K (Figure 3).[40] The *svdWro* value is at a minimum when the oxygen atom is at the 100 K position shown in Figure 1. The *svdWro* values qualitatively track the potential energy of the oxygen position; the expected positions are those observed: the single position at 100 K and an additional alternate oxygen position at the local minimum observed at 293 K. A qualitative indication of the barrier to rotation of the NO is given by the *svdWro* values. Clearly, the barrier to NO rotation is less at 293 K than at 100 K. Since the positions of all of the atoms except the oxygen atom are frozen, no accommodation of the structure to a new oxygen atom position is allowed, and some small differences in the *svdWro* values that could result from such accommodation are ignored. There are two additional qualitative observations that are suggested by the *svdWro* plots. The first is the apparent width of the minima. The valley width of the global minimum is smaller than those of the local minima at both 100 and 293 K, which is consistent with the apparent larger thermal motion of oxygen atom O1b at 293 K (Figure 1). Second, the plot suggests that there is a preferential pathway for the movement of the oxygen atom from position O1 to O1b at 293 K: clockwise rotation of the NO group from position O1 to O1b in Figures 1 and 2. This also corresponds to a left-to-right movement in the plot of Figure 3.

Several additional crystal structures of *tri*-[Fe(T*p*FPP)(NO)(1-MeIm)] at temperatures up to 350 K have been determined. Values of *svdWro* at each new temperature were determined as before and are plotted in Figure S1 in the Supporting Information. Features common to the two temperatures of Figure 3 are seen over the entire 100 to 350 K range, with the expected

(38) Cambridge Crystallographic Data Centre Web site. http://www.ccdc.cam.ac.uk/products/csd/radii/ (accessed April 20, 2008).
(39) When two oxygen atom positions are observed, the starting point is taken from the major-occupancy position.
(40) In each curve of the type illustrated in Figure 3, we used the atomic coordinates from the structure determined at that temperature. Since some thermal expansion or contraction can be expected, the nonbonded contact sums (*svdWro*) are expected to show some temperature dependence.

Table 1. Populations at NO Orientations 1−3 for Six [Fe(T*p*XPP)(NO)(1-MeIm)] Complexes at Various Temperatures

compound	*T* (K)	exp.[a]	populations 1	2	3
tri-[Fe(T*p*FPP)(NO)(1-MeIm)]	100	1−3	1.000	0	−
	100	2−1	1.000	0	−
	150	2−4	1.000	0	−
	175	2−5	1.000	0	−
	200	2−6	0.965(3)	0.035(3)	−
	224	2−3	0.934(3)	0.066(3)	−
	224	1−2	0.945(3)	0.055(3)	−
	293	2−2	0.819(3)	0.181(3)	−
	293	1−1	0.840(3)	0.160(3)	−
	350	2−7	0.735(5)	0.265(5)	−
mono-[Fe(T*p*FPP)(NO)(1-MeIm)]	100	1−1	1.00	0	−
	125	2−3	1.00	0	−
	150	2−2	0.916(3)	0.084(3)	−
	293	2−1	0.738(5)	0.262(5)	−
[Fe(T*p*OCH_3PP)(NO)(1-MeIm)]	100	1−1	1.00	−	−
	100	2−3	1.00	−	−
	293	2−1	0.801(8)	0.199(8)	−
	330	2−2	0.763(9)	0.237(9)	−
[Fe(T*p*CF_3PP)(NO)(1-MeIm)]	100	1−1	0.940(4)	0.060(4)	−
	290	2−1	0.600(5)	0.400(5)	−
[Fe(TPP)(NO)(1-MeIm)]	100	1−1	0.777(4)	0	0.223(4)
	293	1−2	0.37(3)	0.31(1)	0.31(3)
[Fe(T*p*NO_2PP)(NO)(1-MeIm)]	100	1−1	0.637(6)	0.281(6)	0.073(7)

[a] The first number is crystal number and the second is order of data collection.

temperature dependence of the alternate NO positions becoming more energetically accessible. The positions of the local and global minima remain constant, but the apparent barrier to rotation shows a continual decrease as the temperature is increased. The rotation of NO becomes possible at temperatures greater than ∼175 K; a second oxygen atom position at the local minimum is detectable (3%) at 200 K. The population of the oxygen atom increases as the temperature is increased, consistent with the observed decrease in the barrier and the greater thermal motion. Structural data for *tri*-[Fe(T*p*FPP)(NO)(1-MeIm)] were collected in both ascending and descending order. The oxygen atom populations were reproducible at a given temperature, indicating the reversibility of the solid-state motion. The populations of the NO orientations at each temperature are given in Table 1 and Figure S1.

The two minima seen in Figure 3 are the result of the NO ligand being bracketed by peripheral *p*-fluorophenyl groups from different adjacent molecules. We further examined the nature of the nonbonded contacts by calculating the potential energy using semiempirical nonbonded potential functions as originally outlined by Giglio[25] and expanded by Shmueli and Goldberg.[26] We calculated the intermolecular interactions by pairwise addition of all of the interactions involving the oxygen atom positions and all atoms in contact with the oxygen atoms at distances less than the sum of the van der Waals radii. The results for the 100 and 350 K structures are displayed in Figure 4a. The potential energy plots are similar to the simpler *svdWro* summation plots. An important difference is that the difference between the energies of the two minima at each temperature is apparently smaller. The energy difference at 350 K, a point for subsequent discussion, is 6.2 kJ/mol.

The success of this analysis led us to examine several additional six-coordinate samples. A total of six different compounds involving a total of 23 independent structure determinations at temperatures ranging from 100 to 350 K were used in this study. The NO motion ranges from movement between quite discrete positions to disorder best described by a continuum of positions over an angular range.

The crystal structure of [Fe(T*p*OCH_3PP)(NO)(1-MeIm)] at 100 K also shows a single ordered NO. However, the *svdWro* analysis (Figure S2 in the Supporting Information) suggests that this crystalline species could display a disordered NO at higher temperatures. The *svdWro* analysis suggests two well-defined minima with a smaller NO rotation (∼100°) than in *tri*-[Fe(T*p*FPP)(NO)(1-MeIm)]. Crystal structure determinations at 293 and 330 K confirm this prediction, with the population of the second position being temperature-dependent (see Table 1). The potential energy plots at 100 and 330 K (Figure 4b) show similar behavior but again suggest that the *svdWro* plots exaggerate the barrier between the two oxygen positions. The potential energy plot suggests greater accessibility of the second NO position, and indeed, this second position could actually be best represented by a continuum of NO positions. This is consistent with the extended motion of the second (O1b) position, as shown by the thermal ellipsoids in Figure 5. The study of the [Fe(T*p*OCH_3PP)(NO)(1-MeIm)] complex demonstrates the predictive nature of this solid-state mapping.

A second polymorph of [Fe(T*p*FPP)(NO)(1-MeIm)] showed behavior similar to that of [Fe(T*p*OCH_3PP)(NO)(1-MeIm)] in the solid state. At 100 K, *mono*-[Fe(T*p*FPP)(NO)(1-MeIm)] has a single orientation of NO; the *svdWro* plot is displayed in Figure S3 in the Supporting Information. The potential energy plot (Figure 4c) shows a broad minimum for which the valley becomes broader with increasing temperature.[41]

(41) The potential energy between ∼10 and 60° at 100 K (but not at 293 K) was slightly underestimated because of the neglect of modest oxygen−fluorine interactions.

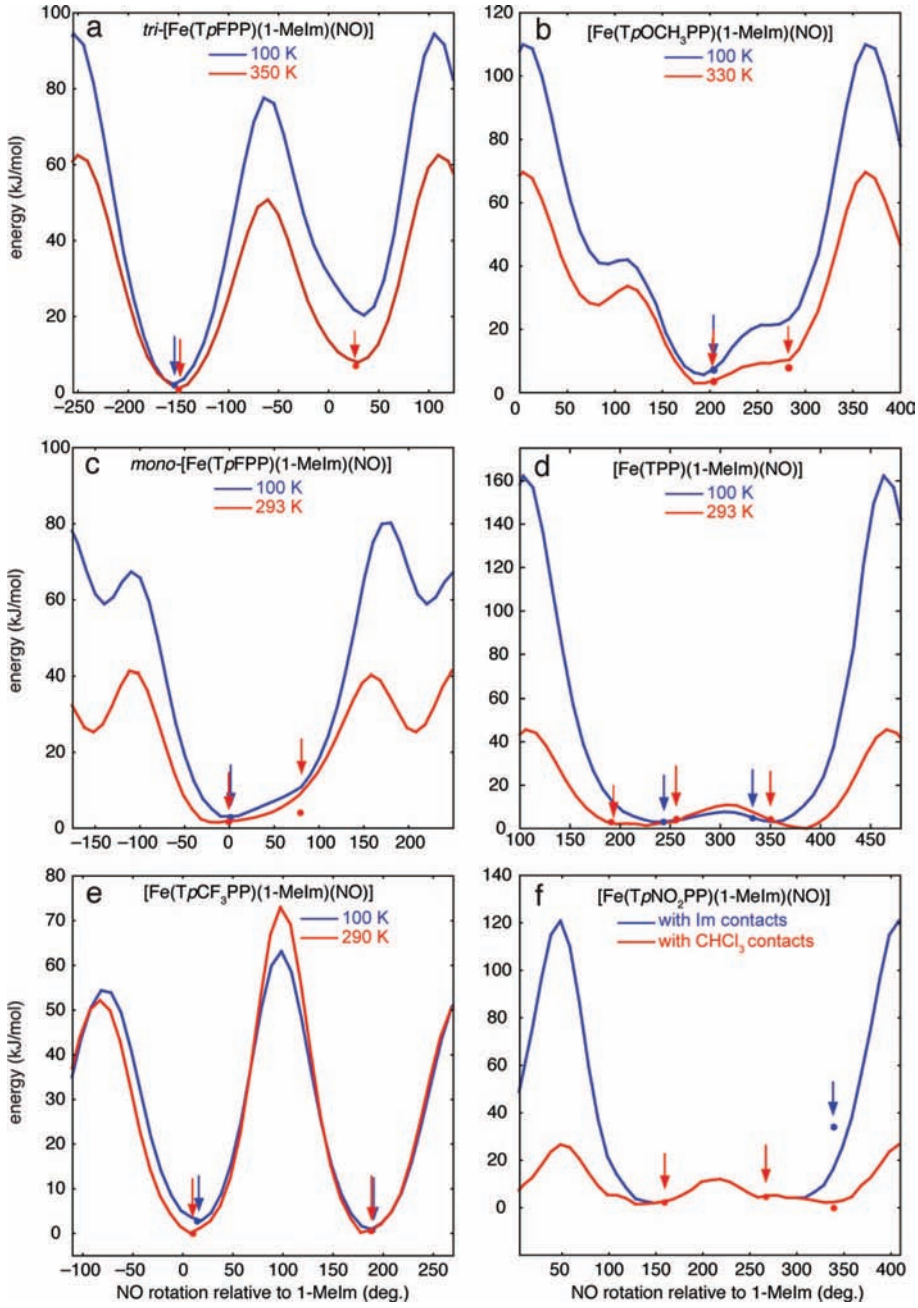

Figure 4. Potential energy diagrams for the six [Fe(Porph)(NO)(1-MeIm) complexes. Values are plotted for the lowest and highest temperatures for which structural data are available. Panel f is at 100 K only. The observed NO positions are shown as points and indicated by arrows.

A second position of NO is populated by a rotation of 70° from the major NO orientation at 150 K but is not observed at 125 K. However, determining a minimal population of oxygen is limited by the detection limits of the X-ray diffraction experiment. This is especially problematic when determining whether a site is unpopulated. In these studies, a 3% (~0.25 electron) occupied oxygen was successfully modeled. More typically, 0.5−1.0 electron (6−12% occupancy) may be confidently found and properly refined.

Unlike the *tri*-[Fe(T*p*FPP)(NO)(1-MeIm)] system, the *mono*-[Fe(T*p*FPP)(NO)(1-MeIm)] system has much less well-defined positions of the NO oxygen atom at temperatures ≥150 K. The 293 K structure of *mono*-[Fe(T*p*FPP)(NO)(1-MeIm)] was refined with the two oxygen positions having equal thermal parameters to better calculate the population of each of the two sites.[24] The complex was also refined with independent thermal parameters for the two oxygen atoms to better observe the unconstrained shape of the thermal ellipsoids. The statistical parameters are similar for both the constrained and unconstrained models. The values of R1 (wR2) for the constrained and unconstrained models are 0.0518 (0.1288) and 0.0514 (0.1282), respectively. An ORTEP diagram of *mono*-[Fe(T*p*FPP)(NO)(1-MeIm)] at 293 K with independent thermal parameters for the two oxygen atoms is given in Figure S7 in the Supporting Information. It is apparent from the elongated thermal ellipsoid of the minor orientation of oxygen (O1b, located at 70°) that there is likely a continuum of unresolved NO positions beginning at or near the position of O1. At temperatures ≤150 K, however, there is only a single, discrete NO orientation (see Figure S7a for the 100 K ORTEP diagram of *mono*-[Fe(T*p*FPP)(NO)(1-MeIm)]).

Next, we analyzed the [Fe(TPP)(NO)(1-MeIm)] system. [Fe(TPP)(NO)(1-MeIm)] is known to have NO rotational

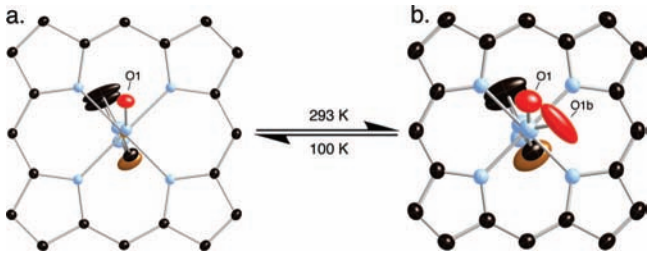

Figure 5. ORTEP diagrams (50% probability ellipsoids) of [Fe(T*p*OCH_3PP)(NO)(1-MeIm)] at (a) 100 and (b) 293 K. The molecules are oriented with the porphyrin plane in the page to emphasize the orientations of NO oxygens. Hydrogen atoms and phenyl rings have been omitted for clarity. The imidazole methyl group is shown as the brown atom.

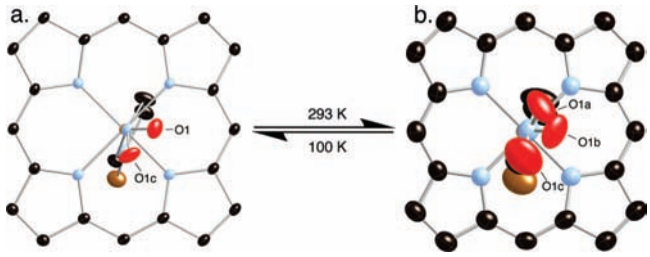

Figure 6. ORTEP diagrams (50% probability ellipsoids) of [Fe(TPP)(NO)(1-MeIm)] at (a) 100 and (b) 293 K. The molecules are oriented with the plane of the porphyrins in the page to emphasize the orientations of NO oxygens. At 100 K, the populations of the O1 and O1c positions are 78 and 22%, respectively. At 293 K, the populations of the O1, O1b, and O1c positions are 38, 31, and 31%, respectively. Hydrogen atoms and phenyl rings have been omitted for clarity. The methyl group of imidazole is shown as the brown atom.

disorder, even at 100 K.[21,22] Both the original [Fe(TPP)(NO)(1-MeIm)] structural data collected at 293 K[21] and the recent structure determination at 100 K[22] display two orientations of the NO ligand. The 100 K structure had NO populations of 85 and 15% and the 293 K structure had NO populations of 67 and 33%. A redetermination of the structure on a single-crystalline sample allowed for a further analysis of the temperature dependence of the NO orientation in [Fe(TPP)(NO)(1-MeIm)]. Additionally, the more extensive data set has provided evidence of a third NO orientation at 293 K. At 100 K, the populations of the NO orientations (78 and 22%) were similar to those reported earlier (see Table 1); however, at 293 K, the structure was better modeled with three NO orientations. The populations of the three orientations, 38, 31, and 31%, agree well with the populations of 67 and 33% observed in the original structure. It should be noted that the 67% position is now modeled as two positions, with occupancies of 38 and 31%.

The *svdWro* plots for [Fe(TPP)(NO)(1-MeIm)] (Figure S4 in the Supporting Information) at the two temperatures are less complex than would be suggested by the crystallographic refinement results. The plots show two distinct minima at each temperature but do not predict the positions of the NO oxygen atoms well. However, the potential energy plot (Figure 4d) shows that there is a broad region where the location of the NO is favorable. This region at 100 K has two very broad minima that become even broader at 293 K. This broadness allows for a range of NO orientations, especially for the two positions nominally described as O1a and O1b (see the ORTEP diagrams in Figure 6). Alternate views of the complete molecule at the two temperatures are given in Figure S8 in the Supporting Information. It is apparent from the thermal ellipsoids of the oxygen atoms at 293 K that there is electron density between the two modeled positions resulting from unresolved NO positions. The statistical parameters were similar for three-position and two-position models at 293 K, with R_1 (wR_2) values of 0.0564 (0.1702) and 0.0569 (0.1723), respectively. Clearly, the nonbonded interactions in [Fe(TPP)(NO)(1-MeIm)] do little to limit the orientations of NO in the crystal.

Like [Fe(TPP)(NO)(1-MeIm)], crystalline [Fe(T*p*CF_3PP)(NO)(1-MeIm)] displays two NO orientations at 100 K, although one site is only slightly populated (0.06 occupancy). However, the temperature-dependent changes in the intermolecular interactions are different from those in the previously analyzed systems. The *svdWro* plots for [Fe(T*p*CF_3PP)(NO)(1-MeIm)] at 100 and 293 K are given in Figure S5 in the Supporting Information. There are two well-defined minima; however, the deeper of the two minima is exchanged on warming. The potential energy plot (Figure 4e) also shows this behavior, with a reversal of the more favorable minimum upon a change in temperature. Clearly, the nonbonded contacts at the ~0° site relax more than those at ~180°. Nonetheless, the differences in the potential energies are relatively small, and the ~0° site is still the minority site for NO occupation. We judge that the temperature-dependent population increase is somewhat larger than those seen in other examples. The two plots suggest that the NO position is rather tightly constrained at both temperatures. This is indeed found experimentally, as can be seen from the ORTEP diagrams shown in Figure S9 in the Supporting Information. Full ORTEP diagrams are given in Figure S10.

Finally, [Fe(T*p*NO_2PP)(NO)(1-MeIm)] was investigated. The nature of the interactions involving the NO ligand in this case is different from that in the previous six-coordinate nitrosyl complexes. Three distinct locations for NO are found, as shown in the ORTEP diagram of Figure S11 in the Supporting Information. However, care must be used in examining the nonbonded interactions of the three NO orientations. The "standard" *svdWro* plot shows that the NO position with the smallest occupancy is apparently strongly disfavored by nonbonded interactions. The nonbonded interactions at this position arise from interactions with a 1-methylimidazole solvate molecule. However, the solvent site is only partly populated by 1-methylimidazole, and a chloroform molecule populates the site 20% of the time. There are no severe nonbonded interactions when the chloroform molecule is present. This is shown in both the *svdWro* plot (Figure S6 in the Supporting Information) and the potential energy plot (Figure 4f), where two distinct potentials have been plotted with the assumption of complete population by either imidazole or chloroform solvate molecules. It is seen that population of the solvent site by chloroform does not lead to unfavorable nonbonded interactions with any of the observed positions of NO, whereas population by imidazole would allow population of only two NO sites. In the event, the occupancy of chloroform [21.0(2)%] is sufficient to allow the observed population of the minor-occupancy NO site. The solvate site is mainly populated by 1-methylimidazole [72(1)%], with a contribution from a second orientation of chloroform that we could not adequately model.

The six [Fe(Porph)(NO)(1-MeIm)] systems allowed us to study the question of whether any preferential orientations of NO and imidazole are discernible. Figures S12−S17 of the Supporting Information provide formal diagrams of the mean planes of the porphyrin cores for all of the derivatives studied at all temperatures. Shown on each diagram are the orientations of both the imidazole and nitrosyl ligands with respect to the porphyrin core. Most species have the major NO orientation

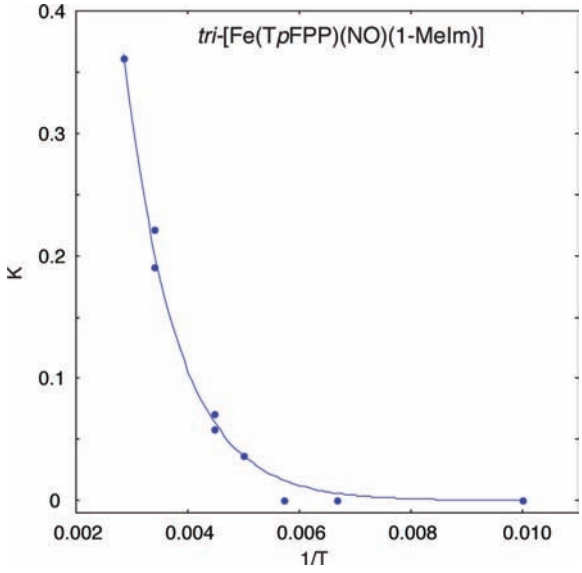

Figure 7. Plot of K vs $1/T$ for *tri*-[Fe(T*p*FPP)(NO)(1-MeIm)]. The equilibrium constants, K, for the transition from the more populated position to the less populated position were calculated from the experimental NO orientation populations, and the data were fit using the van't Hoff equation to determine $\Delta H°$ and $\Delta S°$. The thermodynamic parameters for *tri*-[Fe(T*p*FPP)(NO)(1-MeIm)] are $\Delta H° = 8.9 \pm 0.5$ kJ/mol and $\Delta S° = 17 \pm 1.4$ J mol^{-1} K^{-1}.

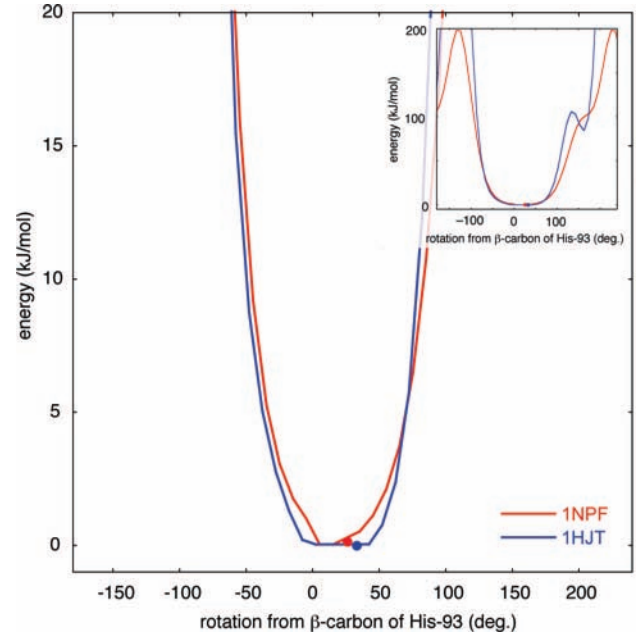

Figure 8. Potential energy vs rotation of the NO oxygen from the β-carbon of His-93 in NOMb, using coordinates from Protein Data Bank entries 1NPF[42] (red) and 1HJT[43] (blue). The observed NO oxygen positions are indicated by the circles.

forming a dihedral angle of 30° or less with the imidazole plane; any secondary orientation shows a wider spread of dihedral angles. There is thus some tendency for the NO and imidazole ligands to have an approximately coplanar arrangement. The observed orientations for [Fe(TPP)(NO)(1-MeIm)] are the obvious exception to the pattern.

Energetics of Solid-State NO Movement. The least-squares-determined populations for the NO oxygen sites in samples with two orientations (see Table 1) were used to determine the thermodynamic parameters for the NO rotation. The equilibrium constant, K, was calculated from the crystallographic populations of the NO orientations at the various temperatures, assuming that all crystallographic measurements represent thermal equilibrium positions:

$$\text{NO major orientation} \overset{K}{\rightleftharpoons} \text{NO minor orientation}$$

The van't Hoff equation (eq 1) was then used to calculate $\Delta H°$ and $\Delta S°$ for rotation of the NO ligand from the major orientation to the minor orientation:

$$\ln K = -\frac{\Delta H°}{RT} + \frac{\Delta S°}{R} \quad (1)$$

Plots of the equilibrium constant versus $1/T$ are given in Figure 7 and Figure S18 in the Supporting Information, and fits to the van't Hoff equation (eq 1) give $\Delta H°$ and $\Delta S°$. The Gibbs free energy, $\Delta G°$, can then be calculated using eq 2:

$$\Delta G° = \Delta H° - T\Delta S° \quad (2)$$

The values found from the fit for *tri*-[Fe(T*p*FPP)(NO)(1-MeIm)] are $\Delta H° = 8.9 \pm 0.5$ kJ/mol, $\Delta S° = 17.2 \pm 1.4$ J mol^{-1} K^{-1}, and $\Delta G° = 3.8$ kJ/mol. It is to be presumed that the small value for $\Delta G°$ reflects the subtle differences in the free energies of the minor and major orientations caused by intermolecular interactions. The $\Delta H°$ value obtained from the fit is close to the value of 6.2 kJ/mol for the difference between the energies of the two minima at 350 K obtained from the potential energy calculation (Figure 4a). Values of $\Delta H°$, $\Delta S°$, and $\Delta G°$ were also obtained from van't Hoff plots for *mono*-[Fe(T*p*FPP)(NO)(1-MeIm)] ($\Delta H° = 4.8 \pm 1.0$ kJ/mol, $\Delta S° = 7.6 \pm 3.7$ J mol^{-1} K^{-1}, and $\Delta G° = 2.3$ kJ/mol) and [Fe(T*p*OCH$_3$PP)(NO)(1-MeIm)] ($\Delta H° = 5.2 \pm 0.5$ kJ/mol, $\Delta S° = 6.1 \pm 1.4$ J mol^{-1} K^{-1}, and $\Delta G° = 3.4$ kJ/mol). Although the two-state population assumption is probably not quite correct for these two systems, the calculations clearly agree with the conclusion that the relative NO orientations have small energy differences.

NO Orientation in Myoglobin. Do these potential energy calculations have any applicability to biological systems? There are two known structures of NOMb, and only a single orientation of NO has been reported for each. Coordinates that are available from the Protein Data Bank, 1NPF[42] and 1HJT,[43] allow an approximate calculation of the potential energy as the oxygen atom is rotated, the results of which are given in Figure 8.[44] Both proteins display a single broad, low-energy region centered around the observed NO position. This minimum is somewhat broader than those seen for *tri*-[Fe(T*p*FPP)(NO)(1-MeIm)] or [Fe(T*p*CF$_3$PP)(NO)(1-MeIm)]. This increased breadth appears to result from our inability to adequately include the contributions from the hydrogen atoms of the amino acids in the ligand binding pocket. A trial calculation for *tri*-[Fe(T*p*FPP)(NO)(1-MeIm)] in which the hydrogen atom contact contributions were neglected confirmed this. We conclude that the ligand binding pocket is effective in limiting the NO ligand in NOMb to a single orientation with NO atom motions comparable to those of *tri*-[Fe(T*p*FPP)(NO)(1-MeIm)] (see Figure 1) or [Fe(T*p*CF$_3$PP)(NO)(1-MeIm)] (see Figure S9 in the Supporting Information). As

(42) Copeland, D. M.; West, A. H.; Ritcher-Addo, G. B. *Proteins: Struct., Funct., Genet.* **2003**, *53*, 182.
(43) Brucker, E. A.; Olson, J. S.; Ikeda-Saito, M.; Phillips, G. N., Jr. *Proteins* **1998**, *30*, 352.
(44) The Protein Data Bank coordinates do not include any hydrogen atom positions.

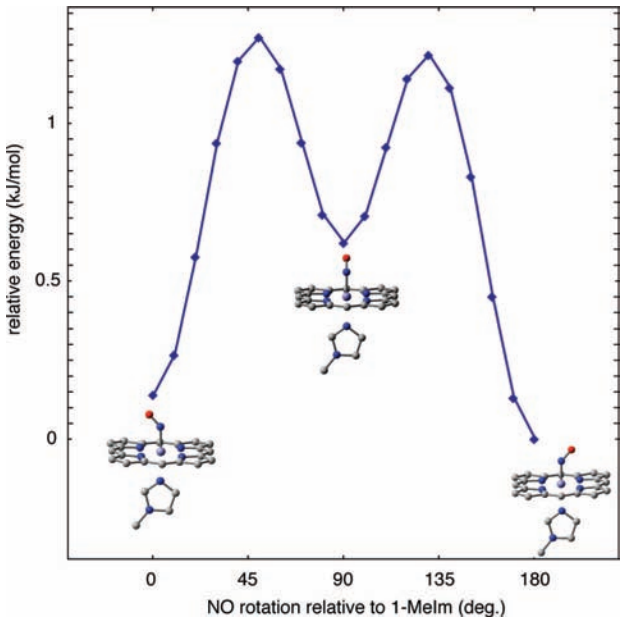

Figure 9. Potential energy landscape calculated using DFT for the [Fe(Porphine)(NO)(1-MeIm)] system. The initial molecular configuration (0°) places the FeNO and 1-MeIm planes coplanar and pointing toward a meso carbon atom. The core conformations of the three energy-minimized structures shown are very similar.

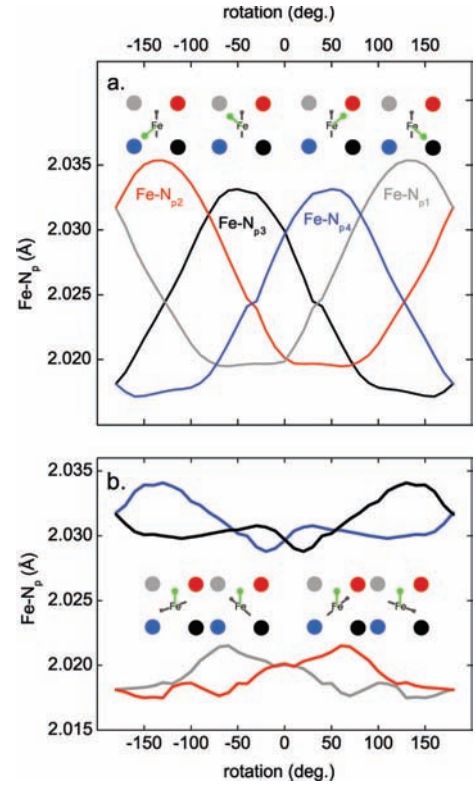

Figure 10. Variation in the lengths of the Fe−N_p bonds versus ligand orientation, based on DFT calculations. The nitrogen atoms are labeled clockwise starting from the upper left as N_{p1}, N_{p2}, N_{p3}, and N_{p4}. At 0°, the FeNO and 1-methylimidazole planes are parallel and the projection of the FeNO plane bisects Fe- N_p1 and Fe- N_p2 (looking down on the porphyrin plane with the NO ligand oriented toward the observer) whereas the 1-methyl group of the 1-methylimidazole plane also bisects Fe−N_{p1} and Fe−N_{p2}. In (a), the NO ligand is rotated with the imidazole orientation held fixed. In (b), the 1-methylimidazole ligand is rotated with the NO orientation held fixed. In both panels, the four porphyrin nitrogen atoms are color coded as shown.

shown in the inset of Figure 8, the protein has a much more tightly defined ligand binding volume than those in the molecular crystals of the six-coordinate nitrosyls.

DFT Calculations. DFT calculations were carried out on an isolated [Fe(porphine)(NO)(1-MeIm)] molecule to explore the energy costs of relative ligand orientations. Calculations were performed to explore the overall energy as NO and imidazole were allowed to take on various orientations with respect to the porphyrin core. In each calculation, either the 1-methylimidazole was placed in a position bisecting a meso carbon and the NO was rotated or the NO was placed in a position bisecting a meso carbon and the 1-methylimidazole was rotated. An energy-minimized structure was calculated for each axial ligand orientation. Because of the many calculations required in the study, the simplified porphine system [Fe(porphine)(NO)(1-MeIm)] was employed. The initial molecular configuration chosen had the FeNO and 1-MeIm planes coplanar and pointing toward a meso carbon atom. This was taken as a position of 0°. The NO group was then rotated from 0 to 360° in 10° intervals, and the energy-minimized structure at each orientation was calculated. The NO and 1-MeIm ligands were held fixed for each rotation, and all of the other parameters were refined freely. As the FeNO group rotates about the Fe−N_{NO} axis, energy maxima are observed when the NO oxygen rotates over an Fe−N_p bond (45 and 135°). Energy minima are observed when the two ligands are coplanar or orthogonal, with a 0.7 kJ/mol increase for the orthogonal orientation. The maximum energy difference for the entire set of relative orientations is only ∼1.5 kJ/mol, as shown in Figure 9. Prior calculations by Patchkovskii and Ziegler[45] on [Fe(porphine)(ImH)(NO)] at the BP86/VWN level of theory using a 45° rotation interval showed a somewhat different energy pattern. In their calculation, the largest energy difference for all orientations was 2.9 kJ/mol, and the differences in the 0° → 90° and 0° → 180° local minima were ∼0 and ∼1.3 kJ/mol, respectively.

The new [Fe(porphine)(NO)(1-MeIm)] calculations suggest an additional subtle effect of relative axial ligand orientation on the bonding parameters at iron. Axial ligand tilt and asymmetry in the equatorial Fe−N_p bonds was first observed experimentally,[22,46,47] where it was always found that the two Fe−N_p bonds that bracket the tilted NO ligand are shorter than the average whereas the other two are longer. This asymmetry is clearly a bonding effect from NO. The electronic basis for the tilt and the equatorial asymmetry was subsequently recognized in several DFT calculations.[48−51] If the NO ligand induces asymmetry, then the asymmetry should be strongly dependent on the NO ligand orientation.

(45) Patchkovskii, S.; Ziegler, T. *Inorg. Chem.* **2000**, *39*, 5354.
(46) Ellison, M. K.; Scheidt, W. R. *J. Am. Chem. Soc.* **1997**, *119*, 7404.
(47) Scheidt, W. R.; Duval, H. F.; Neal, T. J.; Ellison, M. K. *J. Am. Chem. Soc.* **2000**, *122*, 4651.
(48) Leu, B. M.; Zgierski, M. Z.; Wyllie, G. R. A.; Scheidt, W. R.; Sturhahn, W.; Alp, E. E.; Durbin, S. M.; Sage, J. T. *J. Am. Chem. Soc.* **2004**, *126*, 4211.
(49) Praneeth, V. K. K.; Näther, C.; Peters, G.; Lehnert, N. *Inorg. Chem.* **2006**, *45*, 2795.
(50) (a) Ghosh, A.; Wondimagegn, T. *J. Am. Chem. Soc.* **2000**, *122*, 8101. (b) Ghosh, A. *Acc. Chem. Res.* **2005**, *38*, 943.
(51) Cheng, L.; Novozhilova, I.; Kim, C.; Kovalevsky, A.; Bagley, K. A.; Coppens, P.; Richter-Addo, G. B. *J. Am. Chem. Soc.* **2000**, *122*, 7142.
(52) Silvernail, N. J.; Barabanschikov, A.; Pavlik, J. W.; Noll, B. C.; Zhao, J.; Alp, E. E.; Sturhahn, W.; Sage, J. T.; Scheidt, W. R. *J. Am. Chem. Soc.* **2007**, *129*, 2200.

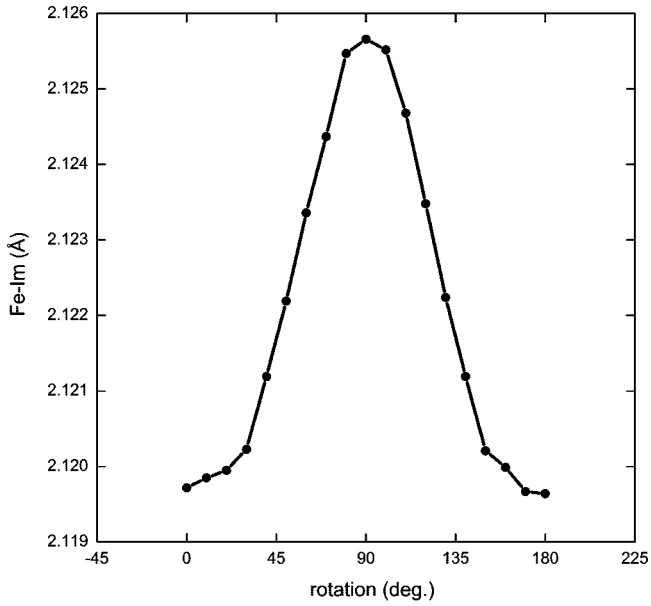

Figure 11. Plot of the $Fe-N_{Im}$ bond length versus NO rotation about the heme normal, from DFT calculations. The angle 0° represents the position where the projections of the FeNO and 1-methylimidazole planes are coplanar, cisoid, and bisecting $Fe-N_{p1}$ and $Fe-N_{p2}$ (looking down on the porphyrin plane with the NO ligand oriented toward the observer).

The dependence of the $Fe-N_p$ bond lengths on varying NO rotational orientation is displayed in Figure 10a. With the rotation starting from 0°, as the FeNO plane is rotated clockwise toward the $Fe-N_{p2}$ bond, the $Fe-N_{p4}$ bond is elongated and the $Fe-N_{p2}$ bond is relatively unchanged. As the FeNO plane is rotated past 90° toward the $Fe-N_{p3}$ bond, the $Fe-N_{p1}$ bond becomes elongated and the $Fe-N_{p3}$ bond is shortened. It should be noted, however, that the elongation of $Fe-N_{p4}$ at 45° is smaller than the elongation of $Fe-N_{p1}$ at 135°. These small differences reflect the subtle effects of the coordinated 1-methylimidazole. Figure 10b displays the changes in the $Fe-N_p$ bonds as the 1-methylimidazole group is rotated around the heme normal with NO fixed. The effects of the 1-methylimidazole rotation are much smaller and overshadowed by the effect of the FeNO plane position on the asymmetry of the porphyrin core.

Finally, the rotation of FeNO around an axis normal to the heme plane has a modest affect on the $Fe-N_{Im}$ bond distance. As the FeNO plane is rotated from 0° (the "cisoid" orientation), the length of the $Fe-N_{Im}$ bond increases. Figure 11 displays the change in the $Fe-N_{Im}$ bond length as the FeNO plane is rotated around the heme normal. At 90°, where the two ligand planes are orthogonal, the $Fe-N_{Im}$ bond length is maximized. The distance is subsequently reduced as NO rotates toward 180° (the "transoid" orientation). These calculations agree quite well with experimental evidence suggesting that the cisoid versus transoid orientations does not affect the $Fe-N_{Im}$ bond length.[52] Although experimental structure determinations first demonstrated the in-plane asymmetry in nitrosyl complexes, some of the effects suggested here on the basis of the DFT calculations are likely smaller than can be observed at the current level of structure determination capabilities.

Summary

The variation in the orientation of the NO ligand in solid-state [Fe(T*p*XPP)(NO)(1-MeIm)] systems has been investigated. Possible orientations of NO result from rotation about the $Fe-N_{NO}$ bond, are controlled by the intermolecular interactions of crystal packing, and can be thermally accessible and reversible. Possible NO orientations can be mapped by calculation of the potential energy differences for all possible orientations of the nitrosyl nitrogen atom in these bent FeNO systems. DFT calculations confirm the low-energy transitions. For the systems considered here, the nonbonded intermolecular interactions dominate the much smaller variations in intramolecular energy predicted by DFT calculations by more than 1 order of magnitude.

Acknowledgment. We thank the National Institutes of Health under Grant GM-38401 (W.R.S.) and the National Science Foundation under Grant PHY-0545787 (J.T.S.) for support of this research. We thank the NSF for X-ray instrumentation support through Grant CHE-0443233.

Supporting Information Available: Complete ref 35; plots of the sum of the van der Waals radii overlaps at all measured temperatures (Figures S1−S6); thermal ellipsoid plots (Figures S7−S11); formal diagrams displaying the perpendicular displacement of core atoms from the 24-atom mean planes at all measured temperatures (Figures S12−S17); plot of K versus $1/T$ (Figure S18); complete crystallographic details, atomic coordinates, bond distances and angles, anisotropic temperature factors, and hydrogen positions for [Fe(TPP)(NO)(1-MeIm)] at 100 and 293 K, [Fe(T*p*CF_3PP)(NO)(1-MeIm)] at 100 and 290 K, and [Fe(T*p*NO_2PP)(NO)(1-MeIm)] at 100 K (Tables S1−S30 and CIF files); and complete details of the DFT calculations for NO and imidazole rotations (Figure S19 and Tables S31 and S32). This material is available free of charge via the Internet at http://pubs.acs.org.

JA8055613